

Particle-In-Cell Simulation of Field-Reversed Configuration with Adaptive Particle Management^{*})

Kento NISHIDA, Xuehan GUO¹⁾, Ritoku HORIUCHI²⁾ and Yasushi ONO¹⁾

Graduate School of Engineering, The University of Tokyo, Tokyo 113-8656, Japan

¹⁾*Graduate School of Frontier Sciences, The University of Tokyo, Chiba 277-8561, Japan*

²⁾*National Institute for Fusion Science, Toki 509-5292, Japan*

(Received 28 December 2017 / Accepted 4 April 2018)

Adaptive Particle Management (APM) method originally developed by Assous is improved for cylindrical 2-dimensional Particle-In-Cell code with 2nd-order shape function. Charge, momentum and energy for overall particles and charge and current density on each grid are rigorously conserved during particle refinements. In order to minimize the deformation of velocity distribution function, phase-space resampling of refinement particles was introduced. We tested our new code in Counter-Helicity Spheromak Merging simulation. Radial shift of X-point during magnetic reconnection is observed, which is consistent with the previously reported result.

© 2018 The Japan Society of Plasma Science and Nuclear Fusion Research

Keywords: Particle-In-Cell, Adaptive Particle Management, cylindrical coordinate, 2nd-order b-spline

DOI: 10.1585/pfr.13.3401060

1. Introduction

Particle-In-Cell (PIC) is a widely used simulation technique which can simulate the non-linear dynamics of plasma such as Field-Reversed Configuration (FRC) [1]. Because finite number of super-particle represent six-dimensional phase space, it can treat kinetic effect economically. If calculation cell does not contain sufficient number of particles, kinetic effect, (e.g. Landau damping), cannot be handled correctly due to low resolution of velocity distribution function (VDF). Therefore, it is desired to have more than 100 particles for each cell. However, when density varies by an order of magnitude, one has to put excessive number of super-particles to express those large densities. In addition, volume element for super-particle varies depending on its radial position in cylindrical geometry. Thus, these density ununiformity make it difficult to use PIC for FRC simulation. FRC has many advantageous features for fusion reactor including high- β , simply connected geometry and natural diverter configuration. Because kinetic effect plays important roles, PIC can be intrinsically attractive simulation for FRC. Here, we introduce weighted particles to resolve density ununiformity problem in FRC. Because it can represent density profile retaining constant number of super-particles in a cell, weighted particles can be efficient technique to treat FRC.

In order to control the number of particles during calculation, several approaches have been proposed. One is based on binary particle splitting and coalescing, originally suggested by Lappenta [2]. Splitting scheme replaces a particle with two equally weighted particles, while co-

alescence scheme combine two particles into one. These scheme can conserve overall mass and either momentum or energy in a cell. If 1st-order shape function is used, charge density on grids is also maintained. One of advantages of Lapenta's scheme is that splitting does not modify VDF because newly generated particles have same velocities as original. On the other hand, coalescence of particles tends to lose high energy fraction of VDF, hence, leads to cooling of plasma. Therefore, a lot of authors paid more attention to coalescence scheme.

Assous *et al.* developed another merging method in 2D triangular cells [3]. This method does not change overall mass, momentum and energy in a cell. In addition, it can also conserve grid moments, namely charge (0th-moment) and current (1st-moment) density. Welch *et al.* extend this method into 2D and 3D cells and demonstrate 2D rectangular cell case [4]. Problems of these grid moments conserved Adaptive Particle Management (APM) method is deformation of VDF. Therefore, several works have focused on preservation of VDF. Teunissen *et al.* improved Lapenta's method by choosing 2 coalescence particles close enough in phase-space using K-d trees [5]. From the same point of view, Vranic *et al.* used 6-dimensional phase-space resampling to find particle pairs [6]. However, these method cannot conserve grid moments rigorously and only suitable for 1st-order shape function.

In this paper, we propose improved particle management scheme based on Assous's method which can be applicable to higher order shape function. Lapenta's splitting scheme is no longer able to conserve charge density with higher order shape function. Thus, We apply Assous's coalescence scheme to both splitting and coalescence scheme, although Assous's method was originally designed for co-

author's e-mail: nishida@ts.t.u-tokyo.ac.jp

^{*}) This article is based on the presentation at the 26th International Toki Conference (ITC26).

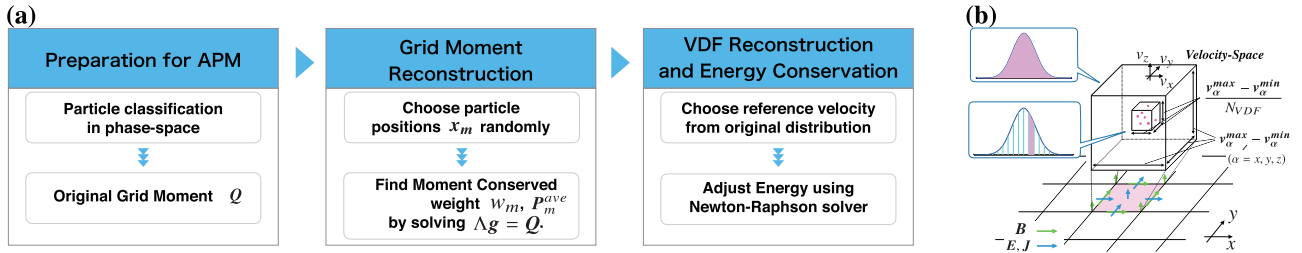


Fig. 1 (a) Overall flow of APM algorithm. (b) Schematic view of staggered grid and 5D-resampling to classify particles in phase-space.

lescence. In order to improve preservation of VDFs and velocity correlations, we also introduce phase-space resampling before APM.

2. Adaptive Particle Management

APM algorithms stated here is based on the method originally outlined by Assous *et al.* [3] and same method by Welch *et al.* [4]. They limit their formulation with the 1st-order shape function. However, it is worth formulating the APM method with higher order scheme. Here we briefly denote their method using 2nd-order shape function.

Assous's method aims to conserve the moments on each node. According to the previous research [3], it is proved that overall particle's moment in a cell will be conserved if the moments on each node are conserved. For example, overall mass M of N particles in a cell ($M = \sum_{n=1}^N w_n m_n$) does not change if the grid moment M_i for i -th grid ($M_i = \sum_{n=1}^N w_n m_n \lambda_i(\mathbf{x}_n)$) is conserved, where w_n, m_n and x_n are weight, mass and position of n -th particle. $\lambda_i(x_n)$ is an interpolation function of particles at position x_m on i -th grid. Thus, it is sufficient to focus on the conservation of grid moments. Figure 1 (a) summarizes the overall flow of refinement algorithm.

Here we consider to control the number of particles in a cell enclosed by full-integer grid preserving grid moments. Then, 2nd-order shape function can distribute particle's weight across 3 grid points on half-integer, and 4 grid points for full-integer grid, respectively. Needless to say, we must use charge conservation method combined with staggered grid to conserve charge density on each grid [7]. Staggered electric field E , magnetic fields B and current density J are defined as shown in Fig. 1 (b). Corresponding to electric field, charge density should be defined on half-integer grid both in x and y coordinate. Therefore, it is required to conserve charge density at 3^2 grid point. At each grid node, charge density Q_i on i -th grid deposited by N particles is given by

$$Q_i = \sum_{n=1}^N w_n \lambda_i(\mathbf{x}_n) \quad (i = 1, 2, \dots, 9). \quad (1)$$

In order to control the number of particles in a cell, let us replace N particles with M particles at positions \mathbf{x}_m and weights w_m . New charge density on each grid can be also written as $Q_i = \sum_{m=1}^M w_m \lambda_i(\mathbf{x}_m)$. For simplicity, we as-

sume the function for new weight $G(\mathbf{x})$ as linear combination of λ_i with coefficients g_j , namely, $w_m = G(\mathbf{x}_m) = \sum_{j=1}^9 g_j \lambda_j(\mathbf{x}_m)$. Then linear equations to be satisfied for moment conservation are given by

$$\sum_{j=1}^9 g_j \sum_{m=1}^M \lambda_j(\mathbf{x}_m) \lambda_i(\mathbf{x}_m) = Q_i. \quad (2)$$

This equations can be denoted in matrix form as $\Lambda g = Q$, where Λ is deposition matrix. This equations can be solved by inverting Λ , and new particle weight w_m can be obtained from g_j . It is known that this method does not ensure the appropriate result. For example, negative weights or some small weighted particles with unreasonably large momentum and energy might be obtained. However, we can avoid these inappropriate reconstruction by adding slight modification in particle position.

1st-order moment (momentum or current density) on the grid can be reconstructed in the same manner. 1st-order moment in x direction on i -th grid P_{xi} is defined on full-integer grid for x and half-integer for y . Hence, it is needed to preserve P_{xi} on $4 \times 3 = 12$ grids. The original 1st-moment of the particle in x on i -th grid is given by

$$P_{xi} = \sum_{n=1}^N w_n P_{xn} \lambda_i(\mathbf{x}_n) \quad (i = 1, 2, \dots, 12). \quad (3)$$

As well as the reconstruction of weight, linear combinations are used to denote the function of new momentum $H(\mathbf{x}) = \sum_{j=1}^{12} h_j \lambda_j(\mathbf{x})$, where h_j is a coefficient for linear combinations. Linear equations for 1st-moment conservation have same form as Eq. (2), namely, $\sum_{j=1}^{12} h_j \sum_{m=1}^M \lambda_j(\mathbf{x}_m) \lambda_i(\mathbf{x}_m) = P_{xi}$. Once coefficients h_j are obtained, h_j gives average x -momentum for m -th particle from $P_{xm}^{ave} = 1/w_m \sum_{j=1}^{12} h_j \lambda_j(\mathbf{x}_m)$. Average velocity in y and z direction are given in the same manner although the number of nodes to be included depends on the position of current. In 2D case, 12 nodes for x and y -direction and 16 nodes for z -direction are needed.

Above procedure gives new particle weight and average velocity conserving original charge and current density on grid. Particles do not have random thermal velocity at this stage, thus, we reconstruct VDF and energy with same manner described by Welch *et al.* For the detail of reconstruction, refer to the original article. In Ref. [4], random momentum p_x^{sam} are sampled by fitted function de-

pending on "peakedness" of original VDF. Because velocities are sampled independently on each direction, correlation between those velocity will totally disappear. In terms of correlation preservation, it is preferred to resample VDF from original particles. However, this method tends to suppress the minority distribution and lead to deformation of VDF. We introduce the 5D-resampling (6D for 3D PIC) for better VDF preservation. Before applying APM stated above, we divide N original particles to be refined into sub-cells in velocity-space. Velocity space between minimum and maximum velocity in $\alpha = x, y, z$ direction, namely, $[v_{\alpha}^{min}, v_{\alpha}^{max}]$ is divided into N_{VDF} sub-cells as shown in Fig. 1 (b). All particles are classified and count the number of particles in each sub-cells. If a sub-cell contains particles more than prescribed threshold, APM will be applied to particles in sub-cells. Because classified particles are close in phase space, it is possible to perform refinement without suppression of minorities. Threshold for APM is determined by the solvability condition of linear equations $\Lambda \mathbf{g} = \mathbf{Q}$. The number of particles M in a sub-cell must be larger than the number of deposition nodes.

3. Result

MHD equilibrium of FRC described in Ref. [8] is used as initial condition for APM test. 144 and 88 particles/cell is set as upper and lower threshold for APM, respectively. Initial weight is given as inverse of volume element. For simplicity, 5D-resampling is not included in this simulation. Figures 2(a), (b) show the distribution of the number of super-particles in a cell N_{ppc} after 100 times APM over 1000 time steps. It is clearly seen that super-particles near the magnetic axis decreases due to APM. Averaged number of super-particles inside and outside the separatrix ($\overline{N_{ppc}^{in}}, \overline{N_{ppc}^{out}}$) are (236.3, 58.9) without APM, while ($\overline{N_{ppc}^{in}}, \overline{N_{ppc}^{out}}$) with APM are (114.1, 109.4). Time evolution of total number of super-particles with various APM intervals are shown in Fig. 2 (c). The more APM routine is called, the faster the number of particles converges. However, Total number of particles converges to 2.52×10^7 and this is equivalent to 124 particles per cell. It is concluded that APM enables to reduce the total number of particles while maintaining sufficient number of particles outside the separatrix.

In order to confirm grid moments and energy conservation, time evolution of error of Poisson's equation and energy deviation are shown in Fig. 3. ΔE_{total} , $\Delta E_{kinetic}$, $\Delta E_{Magnetic}$, $\Delta E_{Electric}$ are deviation of total, kinetic, magnetic and electric energy from initial respective energies. Although APM is performed 1000 times during entire calculation, error of Poisson equation remains quite low (less than error of double precision). Because both charge and current density must be conserved to satisfy Poisson's equation, it is demonstrated that grid moments are well conserved during APM. In addition, total energy is also conserved during APM as shown in Fig. 3 (b).

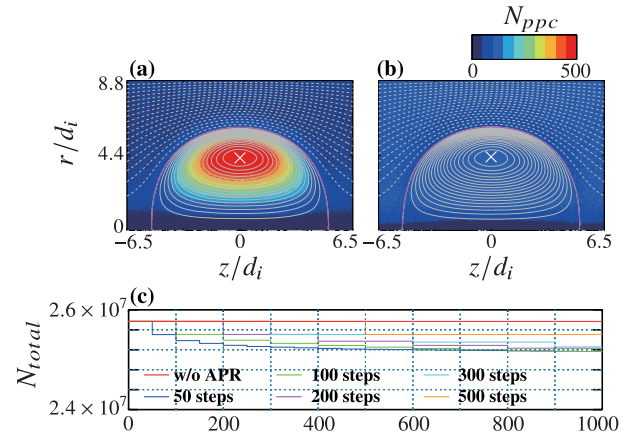


Fig. 2 Colormap of the number of particles (a) without APM (b) with APM at 10 step intervals. White cross and purple line indicate position of magnetic axis and separatrix, respectively. (c) Time evolution of total number of particles for various APM intervals.

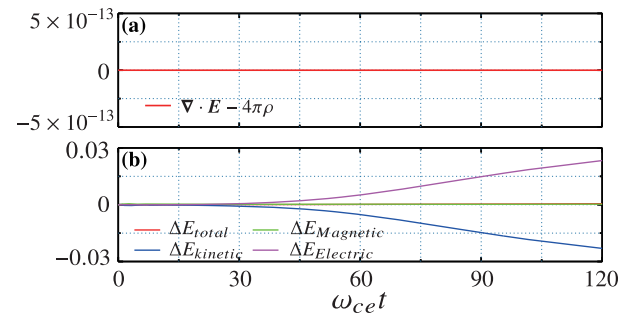


Fig. 3 Time evolution of (a) the number of super-particles for electron (blue), ion (red) and total (green), (b) $\nabla \cdot \mathbf{E} - 4\pi\rho$ (c) deviation of kinetic (blue), electric (purple), magnetic (green) and total energy (red) from initial state.

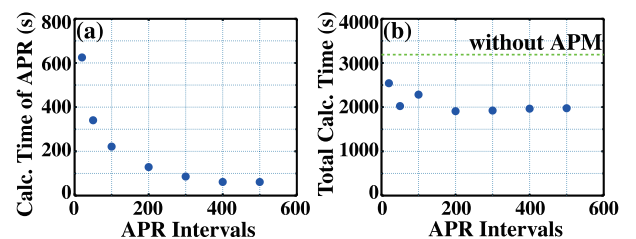


Fig. 4 Calculation time for (a) only APM, (b) entire simulation. Dashed line in (b) shows calculation time without APM.

Although it is not necessary to call the APM routine every time step, frequent APM could be potential computational cost. This is trade off between response speed and computational time. Figure 4 shows the calculation time dependence on APM intervals. It is shown that total calculation time for APM decreases with its interval increase. Calculation time for less APM interval case corresponds to nearly 5% of total calculation time.

Though Assou's method can rigorously conserve charge and current, it potentially modifies VDF. In order

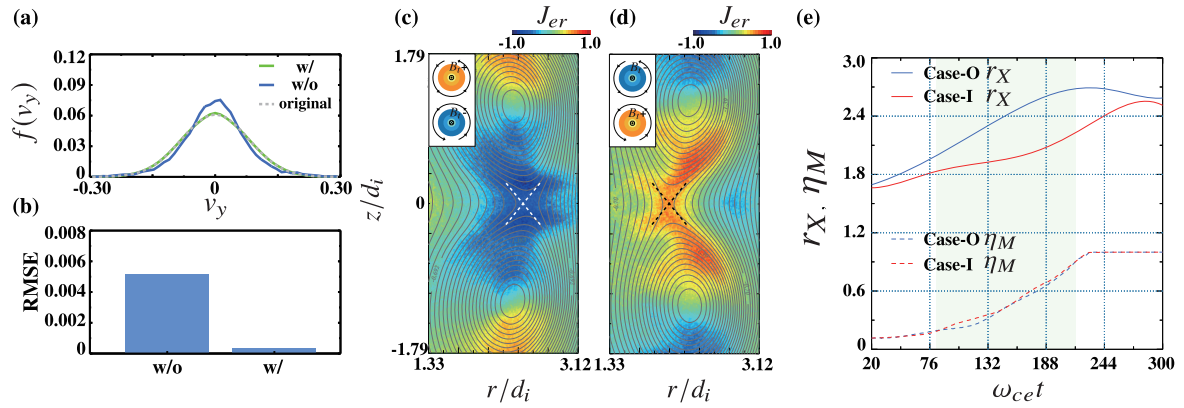


Fig. 5 (a) Velocity distribution function for original particles (dashed gray), with only APM (blue), with APM and 5D-resampling (green). (b) RMSE of VDF with and without 5D-resampling. (c) 2D profiles of radial electron current density (colored) and poloidal magnetic flux (contour lines) during CHSM for Case-O (c) and Case-I (d). Dashed cross indicates the X-point. (e) Radial position of X-point r_X for Case-O (solid blue) and Case-I (solid red). Merging completion rate η_M for Case-O (dashed blue) and Case-I (dashed red). Green shaded region indicate the reconnection duration.

to evaluate the deformation, 500 particles in gaussian distribution are refined with and without 5D-resampling. Figure 5(a) shows VDF deviates from original shape after APM. Without 5D-resampling, distribution function tends to lose higher velocity (minority) fraction, while APM tends to increase majority fraction ($v_y \sim 0$). Therefore, distribution deforms to increase its peakedness. On the other hand, suppressing of minority fraction cannot be seen with 5D-resampling. Root Mean Squared Error (RMSE) in Fig. 5(b) clearly shows 5D-resampling APM causes only slight deformation of VDF. It is effective to suppress minority velocity component to disappear via APM.

Developed Particle-In-Cell code is used to simulate FRC formation by Counter-Helicity Spheromak Merging (CHSM). CHSM is one of formation methods of creating FRC from two separately generated spheromaks via magnetic reconnection. There exist two types of CHSM, called as “Case-I” and “Case-O”, distinguished by combination of poloidal and toroidal magnetic field or polarity of helicity as described in Figs. 5(c), (d). We set two spheromaks with opposite toroidal field and performed weighted particle-In-Cell simulation. It is observed that two initially separated spheromaks gradually approach and relax into a FRC annihilating toroidal field. During magnetic reconnection, X-point movement is observed depending on its polarity of helicity. In Case-O, Outward X-point movement and inward radial electron current is found as shown in Fig. 5(c). On the contrary, X-point depicted as dashed cross in Fig. 5(d) moves radially inward, and the opposite electron radial current density can be seen in Case-I. Time evolution of radial position of X-point r_X and merging completion rate η_M are shown in Fig. 5(e). It shows X-point movement was direct consequence of magnetic reconnection. This is consistent with previously reported phenomenon both in experiment [9] and Hall-MHD simulation [10].

4. Conclusion

In summary, Adaptive Particle Management algorithm for FRC was developed and demonstrated. We extended Assous’s APM algorithm to higher order shape function. It is confirmed that charge and current density on each node are rigorously conserved during APM with 2nd-order shape function. It is shown that total number of particles converges at some levels in later time. Moreover, the response speed depends on the frequency of the management.

PIC simulation of CHSM was performed for the validation of the new algorithm. Previously reported X-point movement were observed depending polarity of the helicity. It is also confirmed that the deformation of VDF is suppressed with newly introduced 5D-resampling technique. It is concluded the number of particles in a cell can be controlled with this APM algorithm.

Acknowledgements

This work was supported by JSPS Fellows No.16J07924.

- [1] C.K. Birdsall and A.B. Langdon, *Plasma Physics Via Computer Simulation* (McGraw-Hill 1985).
- [2] G. Lapenta, *J. Comput. Phys.* **181**, 317 (2002).
- [3] F. Assous, T.P. Dulimbert and J. Segre, *J. Comput. Phys.* **187**, 550 (2003).
- [4] D.R. Welch, T.C. Genoni, R.E. Clark and D.V. Rose, *J. Comput. Phys.* **227**, 143 (2007).
- [5] J. Teunissen and U. Ebert, *J. Comput. Phys.* **259**, 318 (2014).
- [6] M. Vranic, T. Grismayera, J.L. Martinsa, R.A. Fonseca and L.O. Silva, *Comput. Phys. Commun.* **202**, 65 (2016).
- [7] T. ZhEsirkepov, *Comput. Phys. Commun.* **135**, 144 (2001).
- [8] R. Horiuchi, K. Nishimura, T.H. Watanabe and T. Sato, *Nucl. Fusion* **39**, 2083 (1999).
- [9] M. Inomoto, S.P. Gerhardt, M. Yamada, H. Ji, E. Belova, A. Kuritsyn and Y. Ren, *Phys. Rev. Lett.* **97**, 135002 (2006).
- [10] Y. Kaminou, X. Guo, M. Inomoto, Y. Ono and R. Horiuchi, *Phys. Plasmas* **24**, 032508 (2017).